Author Manuscript

Author Manuscript

Author Manuscript

Author Manuscript

HHS Public Access

Author manuscript

ACS Appl Mater Interfaces. Author manuscript; available in PMC 2024 March 29.

Published in final edited form as:

ACS Appl Mater Interfaces. 2023 March 29; 15(12): 15260–15268. doi:10.1021/acsami.3c02640.

Biodegradable Antibacterial Bioorthogonal Polymeric Nanocatalysts Prepared by Flash Nanoprecipitation

Stefano Fedeli[✣,a], **Rui Huang**[✣,a], **Yavuz Oz**[a,b], **Xianzhi Zhang**[a], **Aarohi Gupta**[a], **Sanjana Gopalakrishnan**[a], **Jessa Marie V. Makabenta**[a], **Stephanie Lamkin**[a], **Amitav Sanyal**[b], **Yisheng Xu**[*,c], **Vincent M. Rotello**[*,a]

[a]Department of Chemistry, University of Massachusetts Amherst, 710 North Pleasant Street, Amherst, Massachusetts 01003, United States

[b]Department of Chemistry, Bogazici University, Istanbul 34342, Turkey

[c]State Key Laboratory of Chemical Engineering, East China University of Science and Technology, Shanghai, 200237 P. R. China

Abstract

Bioorthogonal activation of pro-dyes and prodrugs using transition metal catalysts (TMCs) provides a promising strategy for imaging and therapeutic applications. TMCs can be loaded into polymeric nanoparticles through hydrophobic encapsulation to generate polymeric nanocatalysts with enhanced solubility and stability. However, biomedical use of these nanostructures faces challenges due to unwanted tissue accumulation of non-biodegradable nanomaterials and cytotoxicity of heavy metal catalysts. We report here the creation of fully biodegradable nanocatalysts based on an engineered FDA-approved polymer and the naturally existing catalyst hemin. Stable nanocatalysts were generated through kinetic stabilization using flash nanoprecipitation (FNP). The therapeutic potential of these nanocatalysts was demonstrated through effective treatment of bacterial biofilms through the bioorthogonal activation of a pro-antibiotic.

Graphical Abstract

[*]Corresponding Authors: Yisheng Xu, yshxu@ecust.edu.cn; Vincent M. Rotello, rotello@chem.umass.edu.

[✣]These authors contributed equally

Supporting Information

Materials and Methods; Synthesis of polymers; Methods used for Zeta potential, DLS and TEM; Quantification of Hemin loaded in nanocatalysts; Minimum biofilm inhibitory concentration (MBIC) of Cip and pro-Cip.

The authors declare no competing final interest

Author Manuscript Author Manuscript Author Manuscript Author Manuscript

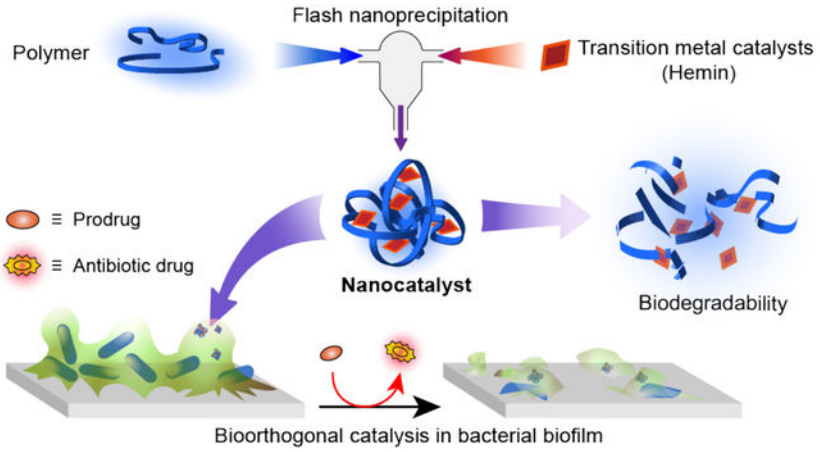

Keywords

Bioorthogonal chemistry; Transition metal catalysts (TMCs); Nanocatalysts; Bioresorbable polymers; Biofilms

INTRODUCTION

Bioorthogonal chemistry represents a class of chemical reactions that are ortogonal to biological transformation, and can take place selectively in biological environments without interfering with endogenous processes.[1–6] Transition metal catalysts (TMCs) are valuable tools for bioorthogonal catalysis, rapidly catalyzing transformations that cannot be achieved by natural enzymes.[7–11] The unmasking reactions of prodrugs mediated by TMCs offer a useful approach for sustained and localized drug generation at the therapeutic site,[12–14] with the potential for efficient treatments with reduced off-target effects.[15–17] The incorporation of TMCs into inorganic nanoparticles enhances solubility and stability of the free catalyst, generating bioorthogonal nanocatalysts that can perform new-to-nature catalysis in living environments.[18,19]

Nanocatalysts protect the catalyst offering a versatile platform to operate in natural systems such as tissues, bacterial biofilms and cells.[20–24] Different nanomaterials have been used to create nanocatalysts,[25,26] including polymers[27,28] gold nanoparticles[29,30] and mesoporous silica.[31,32] However, the applicability of non-biodegradable scaffolds is limited due to the accumulation of nanomaterial in tissues, resulting in chronic inflammatory conditions.[33–35] Moreover, current nanocatalyst platforms rely heavily on the use of heavy metal catalysts such as ruthenium, palladium, and copper, whose possible long-term side effects include hepato-, geno-, and neurotoxicity.[36,37]

In this study, we modified a bioresorbable polylactic-acid (PLA) scaffold to encapsulate TMCs for efficient bioorthogonal catalysis in complex biological environments. PLA is an FDA-approved generally recognized as safe (GRAS) polymer that is fully degraded to lactic acid, a natural metabolite of living systems.[38] PLA isolates and protects the catalyst, mimicking the function of the polypeptide backbone of metalloproteins. Hemin

Author Manuscript Author Manuscript Author Manuscript Author Manuscript

is an iron-containing porphyrin present in the hemoglobin of human blood, and was chosen as the TMC due to its high catalytic activity, biodegradability and biocompatibility.[39] The incorporation of hemin into biodegradable PLA provides a highly biocompatible platform, minimizing the possible nanomaterial accumulation in the body.[40]

Hemin and PLA provide compelling modules for polymeric nanocatalyst design. Incorporation of hemin into hydrophobic PLA polymers is challenging due to the presence of carboxylic moieties on the hemin structure that reduce the hydrophobicity of the porphyrin. Flash nanoprecipitation (FNP) is a versatile nanoparticle production tool that uses rapid micro-mixing to create high supersaturation conditions leading to high solute encapsulation efficiency in polymer-based delivery vehicles.[41] We report here the efficient and reproducible generation of PLA-hemin nanocatalysts using FNP. PLA backbones were synthesized with both hydrophobic and hydrophilic segments, as required for FNP.[42] During FNP, the hydrophobic segments encapsulate solute particles and inhibit their growth, while the hydrophilic segments provide steric stabilization and aqueous stability. The generation of these polymeric nanocatalysts[28] particles was confirmed by dynamic light scattering (DLS) and transmission electron microscopy (TEM). Compared to nanocatalysts generated through conventional precipitation methods,[28] the nanocatalysts prepared by FNP were more stable and have notably higher catalyst loading and enhanced catalytic activity. The degradability of the nanocatalysts was demonstrated by incubating in proteinase-K, with degradation studied by NMR. In living systems, there are several different proteases that can hydrolyze the ester groups of PLA-based polymers.[43] Therefore, we used the ester hydrolyzing enzyme proteinase-K to show the degradation of our PLA-based nanocatalyst.[44] The degradation products of PLA are lactic acid and corresponding oligomers. Lactic acid is a normal intermediate of carbohydrate metabolism and can be readily metabolized, eliminating toxicity from this degradation product.[45] The ability of the nanocatalyst to perform bioorthogonal reactions *in vitro* was first demonstrated with the activation of a pro-dye in bacterial biofilms. The therapeutic potential of these nanocatalysts was then demonstrated through effective treatment of bacterial biofilms by the activation of a pro-antibiotic. The nanocatalyst was eventually tested against mammalian cells, demonstrating the low toxicity of the modified PLA backbone.

RESULTS AND DISCUSSION

2.1 Design and synthesis of the biodegradable nanocatalyst.

The nanocatalysts were generated by encapsulating catalyst molecules into an amphiphilic biodegradable polymer scaffold. Hemin, an endogenously produced porphyrin, was used as the biocompatible TMC.[46,47] Fe-porphyrins efficiently catalyze the reduction of aryl azides to the corresponding amines in the presence of thiols,[48] providing an effective bioorthogonal reaction for the activation of pro-dyes and prodrugs.[49,50] In this catalytic cycle, we used cysteine and ascorbate as cofactors to convert the intermediate Fe^{IV}-nitrene to the reduced amine.[51]

The PLA polymer backbone was engineered with sidechains featuring three essential components: (i) an alkyl chain to provide a hydrophobic inner shell to encapsulate TMCs, (ii) a tetra(ethylene glycol) segment as a spacer to enhance colloidal stability, (iii) a cationic

Author Manuscript Author Manuscript Author Manuscript Author Manuscript

terminal group to maintain water solubility and facilitate interactions with negatively charged bacterial biofilms (Figure 1).[52–54]

The nanocatalysts were prepared by FNP,[55] a scalable process that uses fast mixing conditions to produce a high supersaturation state that stabilizes insoluble, low molecular weight compounds into nanosized polymer particles.[56] In this process, the hydrophobic segment of the sidechains interacts strongly with the lipophilic catalyst, resulting in high adsorption and encapsulation of catalyst molecules.

2.2 Comparison between traditional nanoprecipitation process and FNP approach.

We first compared nanocatalysts fabricated by traditional nanoprecipitation (NC_NP) and those generated by FNP (NC_FNP) for their size, catalyst loading, particle stability, and catalytic activity. FNP-generated NC_FNP showed a smaller particle size and narrower size distribution than NC_NP, according to DLS measurements (Figure 2a). FNP provided higher catalyst loading as well, with NC_FNP having a two-fold higher hemin loading than NC_NP (0.10 ± 0.01 and 0.05 ± 0.01 mg catalyst/mg polymer respectively, Figure 2b). The stability of nanocatalysts was defined through changes in size as measured by DLS (Figure 2c). NC_NP presented poor stability with the particle average size increasing from 170 nm to > 600 nm in 8 days. In contrast, NC_FNP was stable, with no observable size change observed for over 30 days.

The catalytic activity of nanocatalysts was quantified through the activation of a rhodamine-based pro-dye (pro-rhodamine) in PBS solution. The pro-dye (Figure 2d) was prepared by converting the commercially available fluorophore rhodamine 110 to a non-fluorescent bis-azido compound through a reported procedure.[51] The catalytic reduction of both azido groups to their corresponding amines released rhodamine molecules, thus enabling a fluorescence readout of the catalytic activity.

The activation of the pro-rhodamine by the nanocatalyst follows a standard Michaelis–Menten kinetic model (Figure S10), and was measured by mixing nanocatalyst (0.19 mg/mL in PBS), cofactors (1mM L-cysteine and 1mM ascorbate), and pro-dye (12 μM) (Figure 2d). The nanocatalyst produced through FNP (NC_FNP) demonstrated significantly higher catalytic activity on a per-nanocatalyst basis as compared to the standard NC_NP. This increased catalytic activity is arises in part due to the increased catalyst loading afforded by FNP (Figure 2b). Taken together, FNP provides smaller nanocatalyst size, higher catalyst loading, higher stability, and enhanced catalytic activity relative to nanocatalysts produced through traditional nanoprecipitation.

2.3 Biodegradability of the nanocatalyst.

The biodegradability of NC_FNP was investigated in the presence of proteinase-K, a PLA-degrading enzyme.[57,58] The experiments were performed adopting a physiologically significant enzyme concentration and following a reported protocol.[59,66] The polymer was dissolved in deuterated PBS and incubated with proteinase-K (6.9 μM) at 37 °C for two days, monitoring the structure by ^{1}H NMR (Figure 3a). The signals at 1.25 ppm correspond to the protons on methyl groups of the PLA backbone, and were diagnostic for the degradation of the structure during the incubation. Substantial sharpening of

Author Manuscript Author Manuscript Author Manuscript Author Manuscript

these proton signals indicated the formation of smaller molecular weight fragments that can rotate freely in solution, including lactic acid monomers and oligomers (Figure 3b). Nanocatalyst biodegradability was studied by incubating NC_FNP (~0.2 mg/mL) in presence of proteinase-K (6.9 μM) at 37 °C in PBS buffer. As expected, the degradation of the PLA scaffold was accompanied by precipitation of the encapsulated hemin (Figure 3c). The catalytic activity of the degraded nanocatalyst was found to be negligible, as anticipated by the precipitation of the free catalyst in aqueous solution (Figure S13)

2.4 Bioorthogonal activation of a pro-dye in bacterial biofilms.

We investigated the bioorthogonality of nanocatalyst activity in bacterial biofilms through the *in situ* activation of pro-rhodamine. The nanocatalyst (0.19 mg/mL) was incubated with 2-day old DsRed-expressing *E. coli* biofilm for 2 h at 37 °C to allow for the internalization of the nanomaterial. The biofilm was then washed three times with PBS followed by the treatment with pro-rhodamine (50 μM) and cofactors (1 mM L-cysteine and 1 mM ascorbate) for 2h to allow for the bioorthogonal pro-dye activation. As a negative control, biofilms were treated with the pro-dye only.

As shown in Figure 4, pro-rhodamine was activated in biofilms in the presence of nanocatalysts and displayed bright fluorescence. Conversely, a minimal amount of fluorescence was observed in the biofilm treated solely with pro-dye, confirming that the red fluorescence was solely derived from the uncaging of the pro-dye by the nanocatalyst.The colocalization of the fluorophore and DsRed-expressing *E. coli* biofilms was observed in the merged channels, indicating the rhodamine distribution throughout the biofilm.

2.5 Bioorthogonal treatment of pathogenic bacterial biofilm.

The therapeutic potential of the NC_FNP was then tested against bacterial biofilms. We carried out the prodrug activation in bacterial biofilms to demonstrate the therapeutic importance of NC_FNP. Ciprofloxacin (Cip), a fluoroquinolone, was chosen as the antimicrobial agent owing to its high therapeutic efficacy and broad-spectrum activity.[60] The prodrug (pro-Cip) was synthesized through a reported procedure[28] by blocking the pharmacophore, the secondary amino group, with a bulky aryl-azido carbamate moiety. This modification prevented the binding between Cip and its two target enzymes, DNA gyrase and topoisomerase IV,[61] resulting in the reduction of antimicrobial activity by more than 100-fold (Figure S14). Nanocatalysts uncaged the prodrug through the reduction of the aryl azide to its respective amine in the presence of the cofactors (cysteine and ascorbate), triggering the degradation of the benzyl carbamate[62,63,64] and releasing the active antimicrobial agent *in situ* (Figure 5a).

E. coli (CD-2) 2-day old biofilms were treated with the nanocatalyst (0.19 mg/mL) at 37 °C for 2h, to allow sufficient internalization of nanocatalysts within the biofilm. The culture media was then removed, followed by washing three times with PBS. Next, biofilms were treated with different concentrations of pro-Cip, in presence of cofactors (1 mM L-cysteine and 1 mM ascorbate) and incubated for 6h to allow bioorthogonal prodrug activation. Biofilms treated with Cip were used as positive controls, while those incubated with prodrug

Author Manuscript Author Manuscript Author Manuscript Author Manuscript

only or prodrug and polymer were used as negative controls. Controls with no treatment and with nanocatalyst only, were also performed (Figure 5b).

Biofilm viability was analyzed using an Alamar Blue assay (Figure 5b). Biofilms treated with both the nanocatalyst and prodrug demonstrated dose-dependent bactericidal activity, essentially identical to the antibiotic alone. The complete restoration of antimicrobial activity indicates that no other reactions consume the prodrug other than bioorthogonal catalytic conversion. In contrast, biofilms incubated with pro-Cip alone or the combination of pro-Cip and polymer demonstrated no significant bacterial toxicity. Results of control groups demonstrated that bioorthogonal catalystsin the polymer nanocatalysts were responsible for the prodrug activation (Figure 5b).

2.5 Cytotoxicity Assessment of Nanocatalyst with Mammalian Fibroblast Cells.

Having investigated the antimicrobial activity of NC_FNP, we next evaluated its biocompatibility in the presence of mammalian cells. Mammalian NIH 3T3 (ATCC CRL-1658) fibroblast cells were treated with various concentrations of the nanocatalysts for 24 h and the cell viability (%) was then quantified by Alamar Blue assay. As shown in Figure 6, no significant change in fibroblast fibroblasts viability was observed at the nanocatalyst concentrations employed for antimicrobial activity. Cell viability experiments were also performed on the degradation products of the nanocatalyst (after incubation with proteinase-k) to exclude any possible side toxicity of the released monomers (Figure S12).

CONCLUSION

In summary a biodegradable nanocatalyst for the treatment of bacterial biofilms was generated utilizing an engineered PLA polymer scaffold to encapsulate hemin through FNP. The nanocatalysts fabricated by FNP had smaller sizes and narrower size distributions than those produced by conventional precipitation techniques. Significantly, FNP provided higher catalyst loading capacity with concomitantly higher catalytic activity as compared to nanocatalysts produced through standard precipitation. Nanocatalysts were stable in solution but readily degradable by enzymes. The nanocatalyst effectively activated pro-dyes and prodrugs bioorthogonally, showing high antimicrobial activity within biofilms at concentrations harmless to mammalian cells. Overall, this biodegradable nanocatalyst provides a platform for bioorthogonal antimicrobial therapies, with broad potential for other biomedical applications.

EXPERIMENTAL SECTION

Synthesis of polymers.

The PLA-based polymer was synthesized following a reported procedure[65,66] from the comonomers of lactide and furan-protected maleimide-functionalized carbonate, through ring opening polymerization. Maleimide groups were then deprotected and post-functionalized with thioalkyl tetra(ethyleneglycol) trimethylammonium.[67] The resulting polymer was water soluble, characterized by nuclear magnetic resonance (^{1}H-NMR of polymers in Figures S1–S2).

Author Manuscript Author Manuscript Author Manuscript Author Manuscript

Nanocatalyst fabrication.

For the FNP preparations the PLA-based polymer and the catalysts solutions were mixed in the FNP chamber (scheme in Figure 1). Briefly, each mixer inlet was connected to a 1 mL of all-plastic syringe. For mixing, 0.6 mL of 1 mg/mL hemin dissolved in tetrahydrofuran (THF) was loaded in one syringe while 0.6 mL of 1 mg/mL polymer dissolved in water was loaded in another. Next, the two streams were manually impinged at a high velocity inside the mixer chamber. The outlet of the mixer was connected to a vial containing 5 mL of H_2O to further dilute the nanoparticles. The nanocatalyst solution appeared as a yellow-green solution and was subsequently centrifuged 5 times (Amicon® filter, MWCO 10 kDa) to remove any unbound catalyst. The nanocatalyst was characterized by DLS, TEM and zeta potential (Figures S3–S5 respectively). Data confirmed the formation of a stable cationic nanocatalyst (size: ~13 nm, zeta potential: +15 mV). The amount of hemin encapsulated into the polymer nanoparticles (0.10 ± 0.01 mg/mg polymer) was measured by UV-vis (Figure S9).

Evaluation of the catalytic activity of nanocatalysts.

The nanocatalyst solution (0.19 mg/mL in PBS) cofactors (1mM L-cysteine and 1mM ascorbate), and pro-rhodamine (12 μM) were mixed in a 96-well black plate (final volume: 100 μL/well). Fluorescence activation (λ_{ex} = 488 nm, λ_{em} = 521 nm) was recorded immediately after mixing the reagents with a Spectramax M2 microplate reader. Nanocatalyst (with cofactors) and pro-rhodamine (with cofactors) were used as negative controls.

Activation of pro-dye in bacterial biofilms.

DsRed-expressing *E. coli* biofilms were prepared by culturing bacteria in lysogeny broth solution at 37 °C until they reached a stationary phase. 100 μL seeding solutions (0.1 OD_{600}) were added to microplate wells. Next, the microplates were put under static conditions for 2 days at 25 °C. The resulting biofilms were washed with PBS solution three times to remove any adhering planktonic bacteria. Fresh media containing 0.19 mg/mL nanocatalysts was added to the microplates at 37 °C for 2h, to allow sufficient internalization of nanocatalysts within the biofilm. The culture media was then removed, followed by washing three times with PBS. Next, biofilms were treated with pro-rhodamine (50 μM) and incubated for 2h to allow for the bioorthogonal pro-dye activation. The biofilm treated with pro-rhodamine only was used as negative control. Cofactors (1mM L-cysteine and 1mM ascorbate) were present in all the experiments and were added at the timepoint of the pro-rhodamine administration.

Activation of prodrug in bacterial biofilms.

E. coli (CD-2) biofilms were prepared by culturing bacteria in lysogeny broth solution at 37 °C until they reached a stationary phase. 100 uL seeding solutions (0.1 OD_{600}) were added to microplate wells. Next, the microplates were put under static conditions for 2 days at 25 °C. The resulting biofilms were washed with PBS solution three times to remove any adhering planktonic bacteria. Fresh media containing 0.19 mg/mL nanocatalyst was added to the microplates at 37 °C for 2h, to allow sufficient internalization of the nanocatalyst within the biofilm. The culture media was then removed, followed by washing three times with

Author Manuscript Author Manuscript Author Manuscript Author Manuscript

PBS. Next, biofilms were treated with different concentrations of prodrug and incubated for 6h to allow bioorthogonal prodrug activation. Biofilms treated with Cip were used as positive controls, while those incubated with prodrug only or prodrug and polymer were used as negative controls. Nanocatalyst alone and prodrug alone were used as negative controls while drug only was used as positive control. Cofactors (1mM L-cysteine and 1mM ascorbate) were present in all the experiments and were added at the timepoint of Cip/pro-Cip administration. After the incubation, Alamar Blue assay was used to determine the viability of the treated biofilms.

Minimum biofilm inhibitory concentration (MBIC) of Cip and pro-Cip toward *E. coli* (CD-2).

We used an established protocol with minor modifications to test MBICs of the materials used in the studies.[68] Briefly, *E. coli* bacteria (CD-2) were inoculated at 37 °C in TSB broth (2.5 mL/tube) until 0.5 McFarland standard. Then, 150 μL of this solution was seeded onto each well of a 96 well plate with pegged lid, covered and cultured in a shaker at 50 rpm for 5h at 37 °C. Upon completion, the pegged lid was washed by transferring it onto a plate containing 200 μL PBS for 30 secs. The lid was then introduced onto another plate containing 200 μL of pro-Cip or Cip solution dissolved in M9 medium and incubated for 22 h at 37 °C. MBICs were measured using optical density at 600 nm (data presented in Figure S14).

Cell viability study.

NIH 3T3 cells (10 k) were plated in a 96-well plate 24h before the experiment. Cells were washed with PBS and incubated with fresh cell culture media containing different concentrations of nanocatalyst (0.00–0.25 mg/mL) for 24h. Cell viability was determined by Alamar Blue assay after the incubation.

Supplementary Material

Refer to Web version on PubMed Central for supplementary material.

ACKNOWLEDGMENT

This research was supported by the National Institutes of Health EB022641 and AI134770.

REFERENCES

1. Nabawy A; Huang R; C. Luther D; Zhang X; Li C-H; Marie Makabenta J; M. Rotello V All-Natural Gelatin-Based Bioorthogonal Catalysts for Efficient Eradication of Bacterial Biofilms. Chem.Science 2022, 13, 12071–12077
2. Gupta A; Das R; Makabenta JM; Gupta A; Zhang X; Jeon T; Huang R; Liu Y; Gopalakrishnan S; Milán R-C; Rotello VM Erythrocyte-Mediated Delivery of Bioorthogonal Nanozymes for Selective Targeting of Bacterial Infections. Materials Horizons 2021, 8 (12), 3424–3431. [PubMed: 34700339]
3. Zhang X; Lin S; Huang R; Gupta A; Fedeli S; Cao-Milán R; Luther DC; Liu Y; Jiang M; Li G; Rondon B; Wei H; Rotello VM Degradable ZnS-Supported Bioorthogonal Nanozymes with Enhanced Catalytic Activity for Intracellular Activation of Therapeutics. Journal of the American Chemical Society 2022, 144 (28), 12893–12900. [PubMed: 35786910]

Author Manuscript Author Manuscript Author Manuscript Author Manuscript

4. Zhang X; Liu Y; Gopalakrishnan S; Castellanos-Garcia L; Li G; Malassiné M; Uddin I; Huang R; Luther DC; Vachet RW; et al. Intracellular Activation of Bioorthogonal Nanozymes through Endosomal Proteolysis of the Protein Corona. ACS Nano 2020, 14 (4), 4767–4773. [PubMed: 32227914]
5. Hirschbiegel C-M; Fedeli S; Zhang X; Huang R; Park J; Xu Y; Rotello VM Enhanced Design of Gold Catalysts for Bioorthogonal Polyzymes. Materials 2022, 15 (18), 6487. [PubMed: 36143797]
6. Wang W; Zhang X; Huang R; Hirschbiegel C-M; Wang H; Ding Y; Rotello VM In Situ Activation of Therapeutics through Bioorthogonal Catalysis. Adv. Drug Deliv. Rev 2021, 176, 113893. [PubMed: 34333074]
7. Rebelein JG; Ward TR In Vivo Catalyzed New-to-Nature Reactions. Curr. Opin. Biotechnol 2018, 53 (ii), 106–114. [PubMed: 29306675]
8. Hardie J; Makabenta JM; Gupta A; Huang R; Cao-Milán R; Goswami R; Zhang X; Abdulpurkar P; Farkas ME; Rotello VM Selective Treatment of Intracellular Bacterial Infections Using Host Cell-Targeted Bioorthogonal Nanozymes. Materials Horizons 2022, 9 (5), 1489–1494. [PubMed: 35293903]
9. Zhang X; Landis RF; Keshri P; Cao-Milán R; Luther DC; Gopalakrishnan S; Liu Y; Huang R; Li G; Malassiné M; et al. Intracellular Activation of Anticancer Therapeutics Using Polymeric Bioorthogonal Nanocatalysts. Adv. Healthc. Mater 2021, 10 (5), 2001627.
10. Han Y; Gao S; Zhang Y; Ni Q; Li Z; Liang X-J; Zhang J Metal-Based Nanocatalyst for Combined Cancer Therapeutics. Bioconjug. Chem 2020, 31 (5), 1247–1258. [PubMed: 32319762]
11. Wang W; Zhang X; Huang R; Hirschbiegel C-M; Wang H; Ding Y; Rotello VM In Situ Activation of Therapeutics through Bioorthogonal Catalysis. Advanced Drug Delivery Reviews 2021, 176, 113893. [PubMed: 34333074]
12. Fedeli S; Im J; Gopalakrishnan S; Elia JL; Gupta A; Kim D; Vincent M Rotello VM Nanomaterial-based bioorthogonal nanozymes for biological applications. Chem. Soc. Rev 2021, 50, 13467–13480. [PubMed: 34787131]
13. Ortega-Liebana MC; Porter NJ; Adam C; Valero T; Hamilton L; Sieger D; Becker CG; Unciti-Broceta A Truly-Biocompatible Gold Catalysis Enables Vivo-Orthogonal Intra-CNS Release of Anxiolytics. Angew. Chemie Int. Ed 2022, 61, e202111461.
14. Bray TL; Salji M; Brombin A; Pérez-López AM; Rubio-Ruiz B; Galbraith LCA; Patton EE; Leung HY; Unciti-Broceta A Bright Insights into Palladium-Triggered Local Chemotherapy. Chem. Sci 2018, 9 (37), 7354–7361. [PubMed: 30542538]
15. Völker T; Dempwolff F; Graumann PL; Meggers E Progress towards Bioorthogonal Catalysis with Organometallic Compounds. Angew. Chemie Int. Ed 2014, 53 (39), 10536–10540.
16. Völker T; Meggers E Transition-Metal-Mediated Uncaging in Living Human Cells-an Emerging Alternative to Photolabile Protecting Groups. Curr. Opin. Chem. Biol 2015, 25, 48–54. [PubMed: 25561021]
17. Li C-H; Huang R; Makabenta JM; Schmidt-Malan S; Patel R; Rotello VM In Situ Generation of Antibiotics Using Bioorthogonal “Nanofactories.” Microbiol. Insights 2021, 14, 1178636121997121. [PubMed: 33707951]
18. Zhang X; Fedeli S; Gopalakrishnan S; Huang R; Gupta A; Luther DC; Rotello VM Protection and Isolation of Bioorthogonal Metal Catalysts by Using Monolayer-Coated Nanozymes. ChemBioChem 2020, 21 (19), 2759–2763. [PubMed: 32400081]
19. Jeong Y; Tonga GY; Duncan B; Yan B; Das R; Sahub C; Rotello VM Solubilization of Hydrophobic Catalysts Using Nanoparticle Hosts. Small 2018, 14 (7), 1702198.
20. Luther DC; Huang R; Jeon T; Zhang X; Lee Y-W; Nagaraj H; Rotello VM Delivery of Drugs, Proteins, and Nucleic Acids Using Inorganic Nanoparticles. Adv. Drug Deliv. Rev 2020, 156, 188–213. [PubMed: 32610061]
21. Huang R; Luther DC; Zhang X; Gupta A; Tufts SA; Rotello VM Engineering the Interface between Inorganic Nanoparticles and Biological Systems through Ligand Design. Nanomaterials 2021, 11 1001. [PubMed: 33924735]
22. Cao-Milán R; Gopalakrishnan S; He LD; Huang R; Wang L-S; Castellanos L; Luther DC; Landis RF; Makabenta JMV; Li C-H; Zhang X; Scaletti F; Vachet RW; Rotello VM Thermally Gated Bio-

Author Manuscript Author Manuscript Author Manuscript Author Manuscript

Orthogonal Nanozymes with Supramolecularly Confined Porphyrin Catalysts for Antimicrobial Uses. Chem 2020, 1–12.

23. Clavadetscher J; Indrigo E; Chankeshwara SV; Lilienkampf A; Bradley M In-Cell Dual Drug Synthesis by Cancer-Targeting Palladium Catalysts. Angew. Chemie Int. Ed 2017, 56 (24), 6864–6868.
24. Chen J; Li K; Shon JS; Zimmerman SC Single-Chain Nanoparticle Delivers a Partner Enzyme for Concurrent and Tandem Catalysis in Cells. J. Am. Chem. Soc 2020, 142 (10), 4565–4569. [PubMed: 32100539]
25. Chng LL; Erathodiyil N; Ying JY Nanostructured Catalysts for Organic Transformations. Acc. Chem. Res 2013, 46 (8), 1825–1837. [PubMed: 23350747]
26. Prinsen P and Luque R, Chapter 1: Introduction to Nanocatalysts, in Nanoparticle Design and Characterization for Catalytic Applications in Sustainable Chemistry, From the book series: Catalysis Series (RCS books). 2019, pp. 1–36.
27. Bai Y; Feng X; Xing H; Xu Y; Kim BK; Baig N; Zhou T; Gewirth AA; Lu Y; Oldfield E; Zimmerman SC A Highly Efficient Single-Chain Metal-Organic Nanoparticle Catalyst for Alkyne-Azide “Click” Reactions in Water and in Cells. J. Am. Chem. Soc 2016, 138 (35), 11077–11080. [PubMed: 27529791]
28. Huang R; Li C-H; Cao-Milán R; He LD; Makabenta JM; Zhang X; Yu E; Rotello VM Polymer-Based Bioorthogonal Nanocatalysts for the Treatment of Bacterial Biofilms. J. Am. Chem. Soc 2020, 142 (24), 10723–10729. [PubMed: 32464057]
29. Das R; Landis RF; Tonga GY; Cao-Milán R; Luther DC; Rotello VM Control of Intra- versus Extracellular Bioorthogonal Catalysis Using Surface-Engineered Nanozymes. ACS Nano 2019, 13 (1), 229–235. [PubMed: 30516966]
30. Tonga GY; Jeong Y; Duncan B; Mizuhara T; Mout R; Das R; Kim ST; Yeh Y-C; Yan B; Hou S; Rotello VM Supramolecular Regulation of Bioorthogonal Catalysis in Cells Using Nanoparticle-Embedded Transition Metal Catalysts. Nat. Chem 2015, 7 (7), 597–603 [PubMed: 26100809]
31. Wang F; Zhang Y; Du Z; Ren J; Qu X Designed Heterogeneous Palladium Catalysts for Reversible Light-Controlled Bioorthogonal Catalysis in Living Cells. Nat. Commun 2018, 9 (1),1209. [PubMed: 29572444]
32. Destito P; Sousa-Castillo A; Couceiro JR; López F; Correa-Duarte MA; Mascareñas JL Hollow Nanoreactors for Pd-Catalyzed Suzuki–Miyaura Coupling and O -Propargyl Cleavage Reactions in Bio-Relevant Aqueous Media. Chem. Sci 2019, 10 (9), 2598–2603. [PubMed: 30996975]
33. Chandra Sekhara Rao G; Satish Kumar M; Mathivanan N; Bhanoji Rao ME Improvement of physical stability and dissolution rate of celecoxib suspensions by complexation with beta-cyclodextrins. Pharmazie 2004, 59,5–9. [PubMed: 14964413]
34. Popp L; Segatori L Differential Autophagic Responses to Nano-Sized Materials. Curr. Opin. Biotechnol 2015, 36, 129–136. [PubMed: 26340102]
35. Martinez Legaspi S; Segatori L Aggregation Behavior of Nanoparticle-Peptide Systems Affects Autophagy. Bioconjug. Chem 2019, 30 (7), 1986–1997. [PubMed: 31268689]
36. Mello-Andrade F; Cardoso CG; e Silva CR; Chen-Chen L; de Melo-Reis PR; de Lima AP; Oliveira R; Ferraz IBM; Grisolia CK; Almeida MAP; et al. Acute Toxic Effects of Ruthenium (II)/Amino Acid/Diphosphine Complexes on Swiss Mice and Zebrafish Embryos. Biomed. Pharmacother 2018, 107, 1082–1092. [PubMed: 30257320]
37. Egorova KS; Ananikov VP Toxicity of Metal Compounds: Knowledge and Myths. Organometallics 2017, 36 (21), 4071–4090.
38. Tokiwa Y; Calabia BP Biodegradability and Biodegradation of Poly(Lactide). Appl. Microbiol. Biotechnol 2006, 72 (2), 244–251. [PubMed: 16823551]
39. Wang Q; Yang Z; Zhang X; Xiao X; Chang CK; Xu B A Supramolecular-Hydrogel-Encapsulated Hemin as an Artificial Enzyme to Mimic Peroxidase. Angew. Chemie Int. Ed 2007, 46 (23), 4285–4289.
40. Kwon GS; Furgeson DY Biodegradable Polymers for Drug Delivery Systems. In Biomedical Polymers; Jenkins M, Ed.; Woodhead Publishing Series in Biomaterials; Woodhead Publishing, 2007; pp 83–110.

Author Manuscript Author Manuscript Author Manuscript Author Manuscript

41. Huang R; Hirschbiegel C-M; Zhang X; Gupta A; Fedeli S; Xu Y; Rotello VM Engineered Polymer-Supported Bioorthogonal Nanocatalysts Using Flash Nanoprecipitation. ACS Appl. Mater. Interfaces 2022, 14 (28), 31594–31600. [PubMed: 35802797]
42. Markwalter CE; Pagels RF; Wilson BK; Ristroph KD; Prud'homme RK Flash Nanoprecipitation for the Encapsulation of Hydrophobic and Hydrophilic Compounds in Polymeric Nanoparticles. J. Vis. Exp 2019, 2019 (143), 1–13.
43. Madhavan Nampoothiri K; Nair NR; John RP An Overview of the Recent Developments in Polylactide (PLA) Research. Bioresour. Technol 2010, 101 (22), 8493–8501. [PubMed: 20630747]
44. Samarajeewa S; Shrestha R; Li Y; Wooley KL Degradability of Poly(Lactic Acid)-Containing Nanoparticles: Enzymatic Access through a Cross-Linked Shell Barrier. J. Am. Chem. Soc 2012, (134), 1235–1242. [PubMed: 22257265]
45. Pawar RP, Tekale SU, Shisodia SU, Totre JT, Domb AJ Biomedical applications of poly(lactic acid). Recent Pat. Regen. Med 2014, (4), 40–51.
46. Ehrenberg A, in Chance B, & Eestabrook W, and Yonetani T (Editors), Hemes and hemoproteins, Academic Press, New York, 1966, p. 133.
47. Traylor PS; Dolphin D; Traylor TG Sterically Protected Hemins with Electronegative Substituents: Efficient Catalysts for Hydroxylation and Epoxidation. J. Chem. Soc. Chem. Commun 1984, 5, 279–280.
48. Lippert AR; New EJ; Chang CJ Reaction-Based Fluorescent Probes for Selective Imaging of Hydrogen Sulfide in Living Cells. J. Am. Chem. Soc 2011, 133 (26), 10078–10080. [PubMed: 21671682]
49. Sasmal PK; Streu CN; Meggers E Metal Complex Catalysis in Living Biological Systems. Chem. Commun 2013, 49 (16), 1581–1587.
50. Cenini S; Gallo E; Caselli A; Ragaini F; Fantauzzi S; Piangiolino C Coordination Chemistry of Organic Azides and Amination Reactions Catalyzed by Transition Metal Complexes. Coord. Chem. Rev 2006, 250 (11–12), 1234–1253.
51. Sasmal PK; Carregal-Romero S; Han AA; Streu CN; Lin Z; Namikawa K; Elliott SL; Köster RW; Parak WJ; Meggers E Catalytic Azide Reduction in Biological Environments. ChemBioChem 2012, 13 (8), 1116–1120. [PubMed: 22514188]
52. Wang L-S; Gupta A; Rotello VM Nanomaterials for the Treatment of Bacterial Biofilms. ACS Infect. Dis 2016, 2 (1), 3–4. [PubMed: 27622944]
53. Zhang X; Huang R; Gopalakrishnan S; Cao-Milán R; Rotello VM Bioorthogonal Nanozymes: Progress towards Therapeutic Applications. Trends Chem. 2019, 1 (1), 90–98. [PubMed: 34095799]
54. Nabawy A; Makabenta JM; Schmidt-Malan S; Park J; Li C-H; Huang R; Fedeli S; Chattopadhyay AN; Patel R; Rotello VM Dual Antimicrobial-Loaded Biodegradable Nanoemulsions for Synergistic Treatment of Wound Biofilms. Journal of Controlled Release 2022, 347, 379–388. [PubMed: 35550914]
55. Wang M; Xu Y; Liu Y; Gu K; Tan J; Shi P; Yang D; Guo Z; Zhu W; Guo X; Cohen Stuart MA Morphology Tuning of Aggregation-Induced Emission Probes by Flash Nanoprecipitation: Shape and Size Effects on in Vivo Imaging. ACS Appl. Mater. Interfaces 2018, 10 (30), 25186–25193. [PubMed: 29975045]
56. Wang M; Yang N; Guo Z; Gu K; Shao A; Zhu W; Xu Y; Wang J; Prud'homme RK; Guo X Facile Preparation of AIE-Active Fluorescent Nanoparticles through Flash Nanoprecipitation. Ind. Eng. Chem. Res 2015, 54 (17), 4683–4688.
57. Li F; Wang S; Liu W; Chen G Purification and Characterization of Poly(l-Lactic Acid)-Degrading Enzymes from Amycolatopsis Orientalis Ssp. Orientalis. FEMS Microbiol. Lett 2008, 282 (1), 52–58. [PubMed: 18355279]
58. Huang Q; Hiyama M; Kabe T; Kimura S; Iwata T Enzymatic Self-Biodegradation of Poly(L-Lactic Acid) Films by Embedded Heat-Treated and Immobilized Proteinase K. Biomacromolecules 2020, 21 (8), 3301–3307. [PubMed: 32678613]
59. De Tayrac R; Chentouf S; Garreau H; Braud C; Guiraud I; Boudeville P; Vert M In Vitro Degradation and in Vivo Biocompatibility of Poly(Lactic Acid) Mesh for Soft Tissue Reinforcement in Vaginal Surgery. J. Biomed. Mater. Res. B Appl. Biomater 2008, 85B, 529–536.

Author Manuscript Author Manuscript Author Manuscript Author Manuscript

60. Caeiro J-P; Iannini PB Moxifloxacin (Avelox®): A Novel Fluoroquinolone with a Broad Spectrum of Activity. Expert Rev. Anti. Infect. Ther 2003, 1 (3), 363–370. [PubMed: 15482134]

61. Drlica K; Zhao X; DNA gyrase, topoisomerase IV, and the 4-quinolones. Microbiol. Mol. Biol. Rev 1997, 61 (3): 377–92. [PubMed: 9293187]

62. van Brakel R; Vulders RCM; Bokdam RJ; Grüll H; Robillard MS A Doxorubicin Prodrug Activated by the Staudinger Reaction. Bioconjug. Chem 2008, 19 (3), 714–718. [PubMed: 18271515]

63. Matikonda SS; Orsi DL; Staudacher V; Jenkins IA; Fiedler F; Chen J; Gamble AB Bioorthogonal Prodrug Activation Driven by a Strain-Promoted 1,3-Dipolar Cycloaddition. Chem. Sci 2015, 6 (2), 1212–1218. [PubMed: 29560207]

64. O'Connor LJ; Mistry IN; Collins SL; Folkes LK; Brown G; Conway SJ; Hammond EM CYP450 Enzymes Effect Oxygen-Dependent Reduction of Azide-Based Fluorogenic Dyes. ACS Cent. Sci 2017, 3 (1), 20–30. [PubMed: 28149949]

65. Onbulak S; Tempelaar S; Pounder RJ; Gok O; Sanyal R; Dove AP; Sanyal A Synthesis and Functionalization of Thiol-Reactive Biodegradable Polymers. Macromolecules 2012, 45 (3), 1715–1722.

66. Oz Y; Nabawy A, Fedeli S, Gupta A; Huang R, Sanyal A, and Rotello VM Biodegradable Poly(lactic acid) Stabilized Nanoemulsions for the Treatment of Multidrug-Resistant Bacterial Biofilms. ACS Appl. Mater. Interfaces 2021, 13, 34, 40325–40331. [PubMed: 33356095]

67. Li X; Yeh YC; Giri K; Mout R; Landis RF; Prakash YS; Rotello VM Control of Nanoparticle Penetration into Biofilms through Surface Design. Chem. Commun 2015, 51 (2), 282–285.

68. Harrison JJ; Stremick CA; Turner RJ; Allan ND; Olson ME; Ceri H Microtiter Susceptibility Testing of Microbes Growing on Peg Lids: A Miniaturized Biofilm Model for High-Throughput Screening. Nat. Protoc 2010, 5, 1236–1254. [PubMed: 20595953]

Author Manuscript Author Manuscript Author Manuscript Author Manuscript

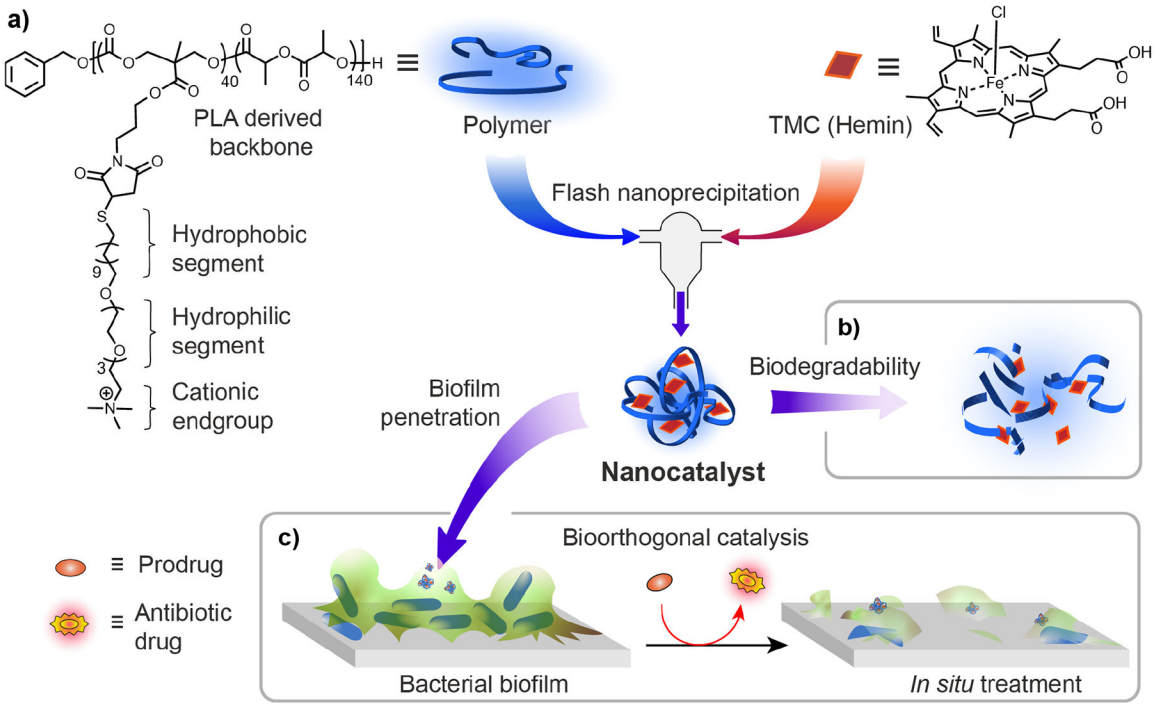

Figure 1.

a) Structures of hemin and polymer nanoparticles. b) Schematic representation of the nanocatalyst degradation. c) Schematic demonstration of the bioorthogonal activation for therapeutics.

Author Manuscript
Author Manuscript
Author Manuscript
Author Manuscript

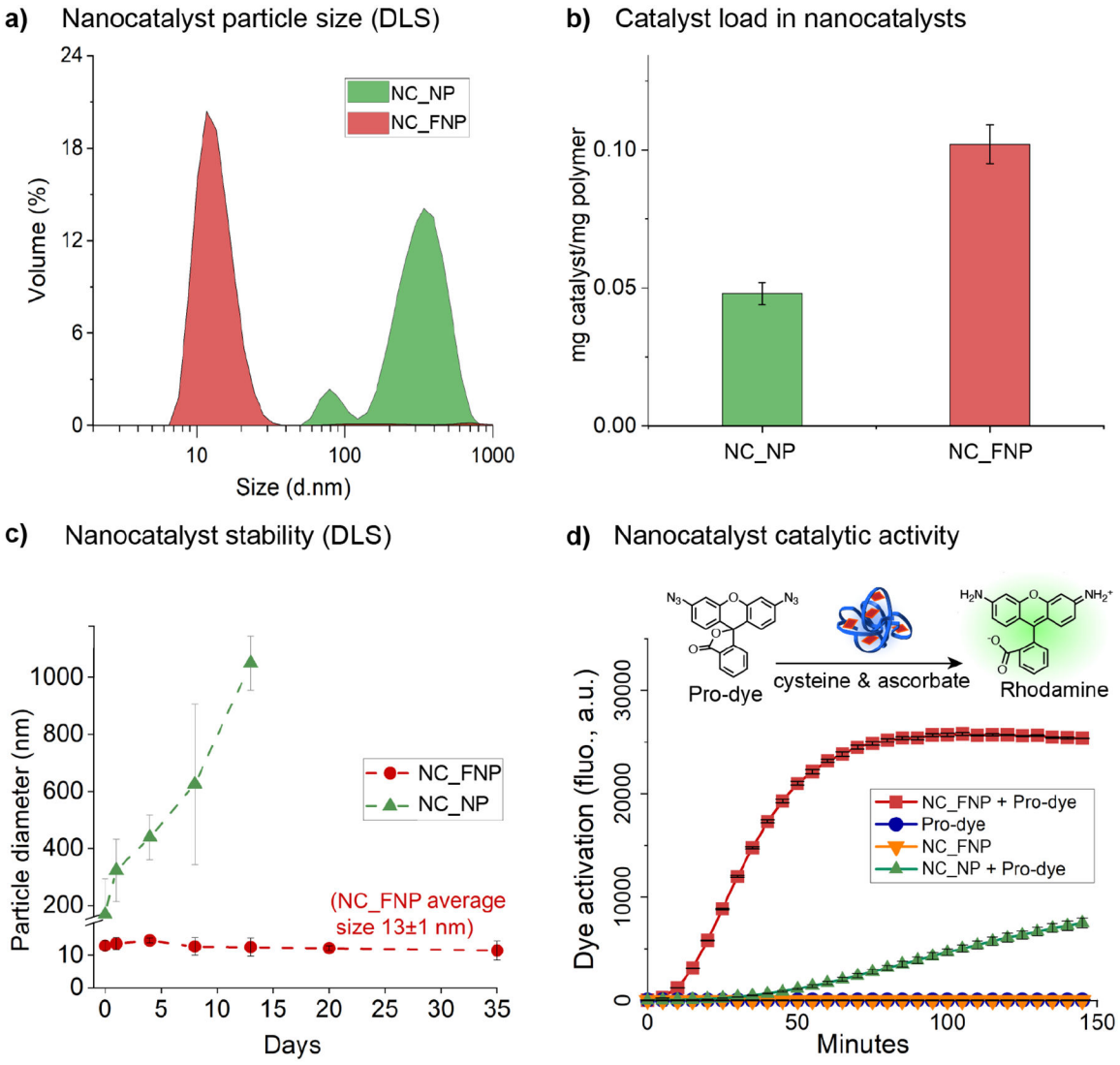

Figure 2.

(a) Size of the nanocatalysts measured with DLS (NC_FNP PDI 0.6; NC_NP PDI 0.7). (b) Quantification of the hemin catalyst loaded in nanocatalysts. (c) Stability of the nanocatalysts in PBS, as measured by DLS. (d) Catalytic activity of nanocatalysts (0.19 mg/mL in PBS) tracked by measuring the fluorescence activation of the pro-dye (λ_{ex} = 488 nm, λ_{em} = 521 nm). Each experiment was repeated three times. For b), c), d), error bars represent the standard deviation.

Author Manuscript Author Manuscript Author Manuscript Author Manuscript

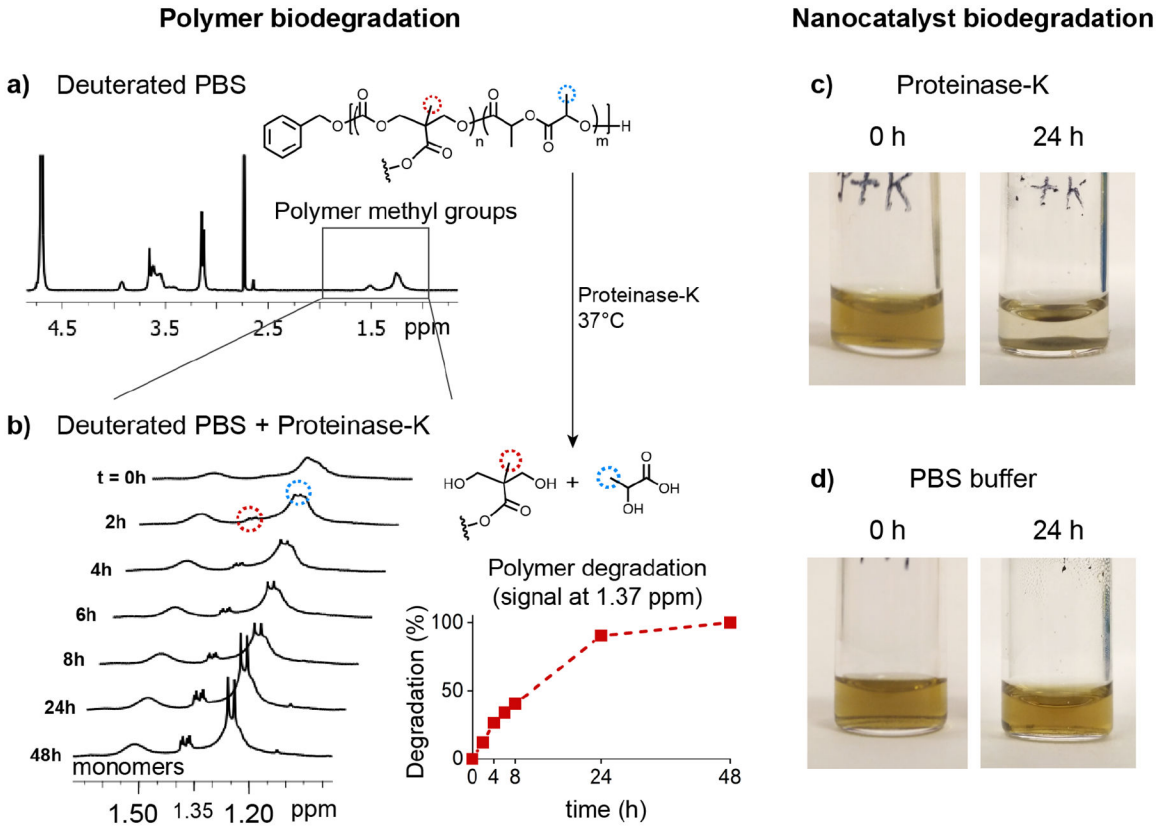

Figure 3.

Biodegradation of the polymer and nanocatalyst in the presence of proteinase-K. a) ^{1}H-NMR spectra of the polymer. b) Degradation kinetics measured by ^{1}H-NMR; the quantification was obtained by integrating the normalized monomer signals over time. c), d) Nanocatalyst incubated at 37 °C with and without proteinase-K, respectively.

Author Manuscript Author Manuscript Author Manuscript Author Manuscript

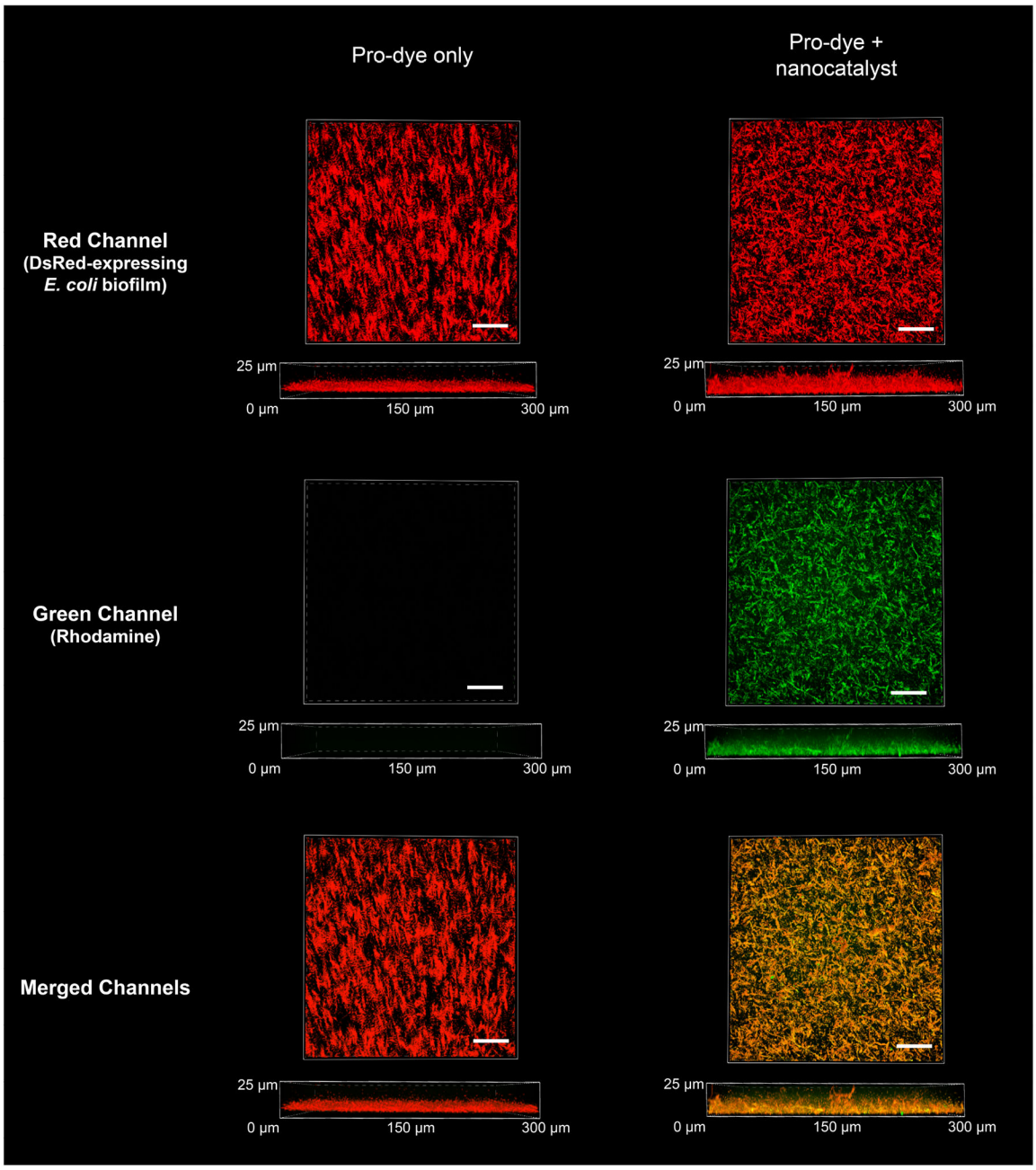

Figure 4.

Confocal microscopy images of DsRed-expressing *E. coli* biofilm incubated with the nanocatalyst followed by treatment with the pro-dye (pro-rhodamine). Squares show the top view of biofilms, while the rectangles below show the corresponding side view. Scale bar = 50 μm.

Author Manuscript Author Manuscript Author Manuscript Author Manuscript

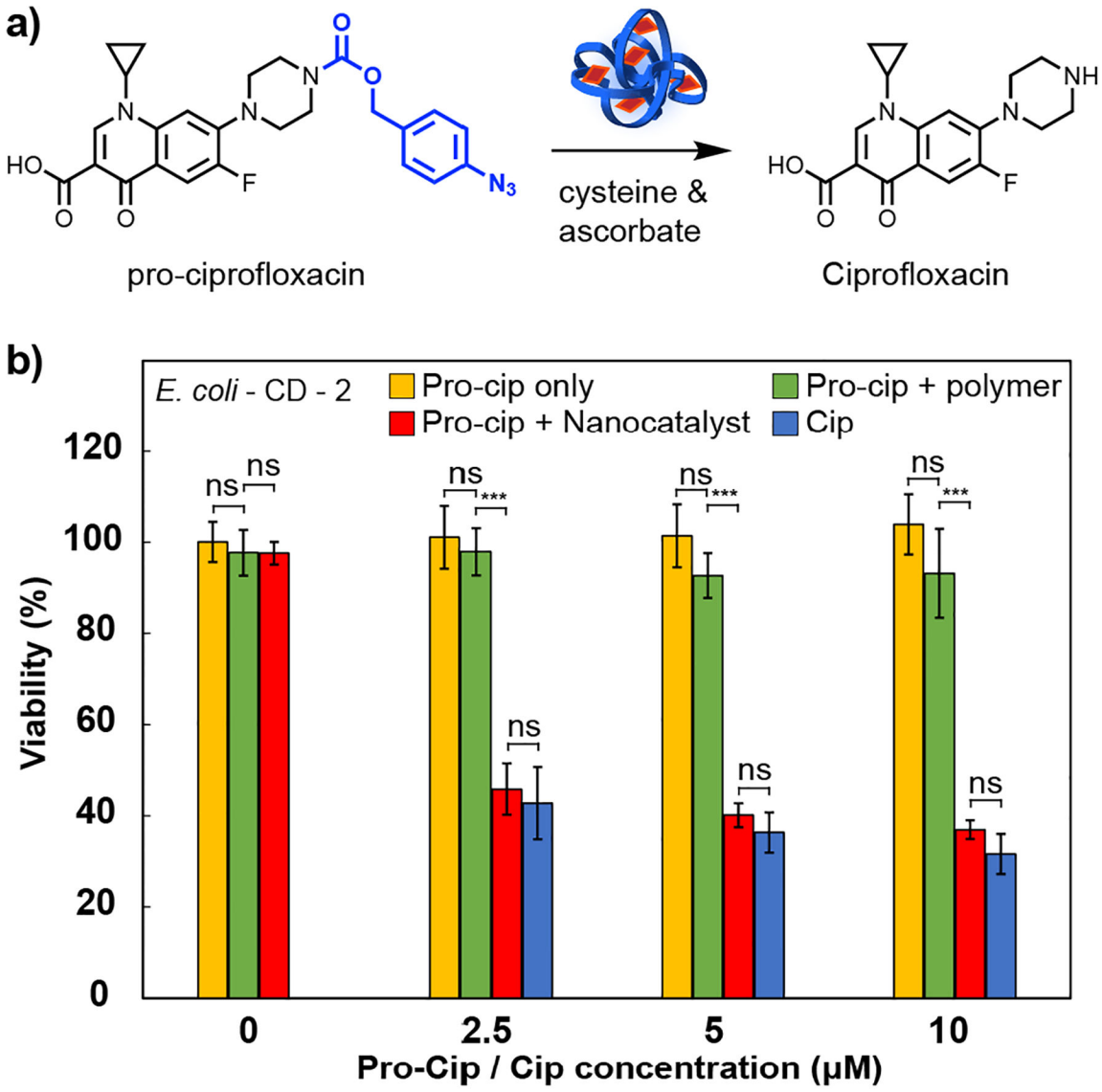

Figure 5.

a) Schematic representation of the activation of pro-ciprofloxacin. b) Viability of *E. coli* (CD-2) biofilms incubated with the nanocatalyst (2h, 0.19 mg/mL) followed by treatment with prodrug (6h). The data at Pro-Cip concentration = 0 represent the control experiments without drug or prodrug; specifically, the yellow, green, and red bars represent polymer alone, no treatment, and nanocatalyst alone respectively. *** = p value < 0.001. Each experiment was repeated three times, error bars represent standard deviation.

Author Manuscript Author Manuscript Author Manuscript Author Manuscript

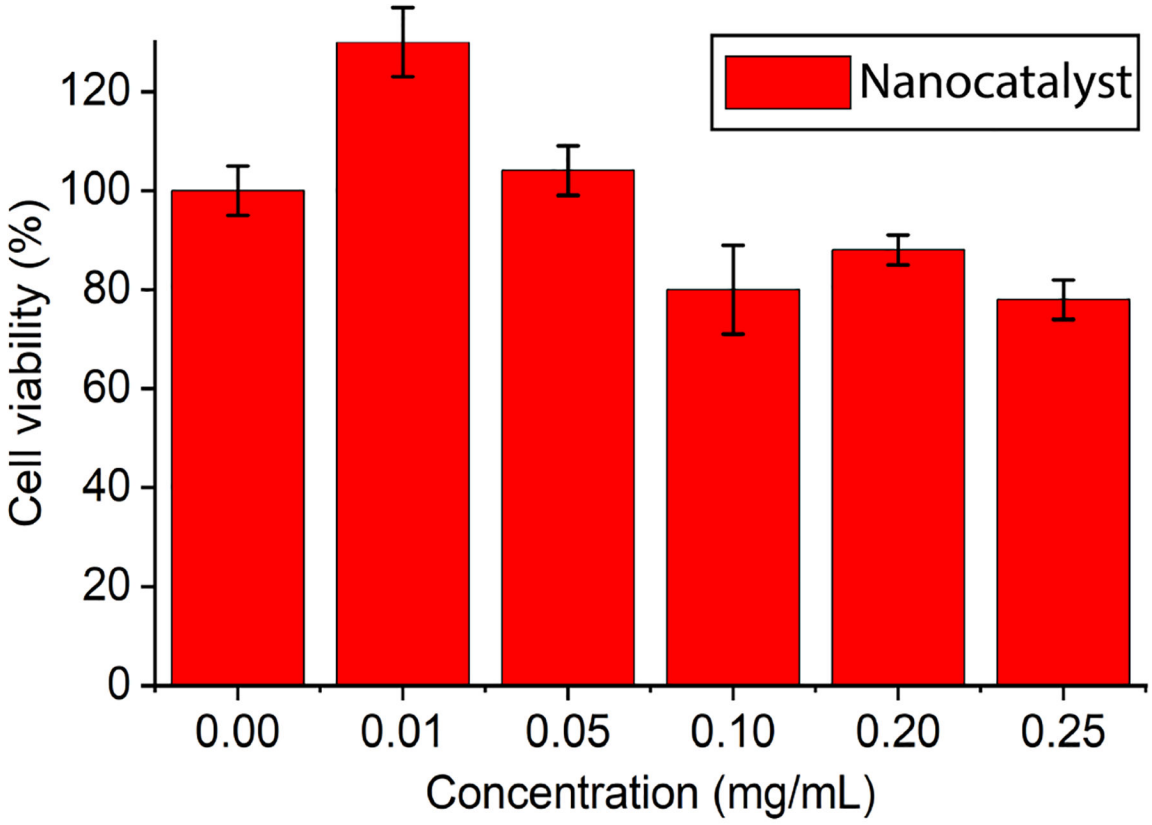

Figure 6.
Fibroblast viability after treating with nanocatalyst NC_FNP for 24 h. Each experiment was repeated three times, error bars represent the standard deviations.